Proceedings of the ASME 2010 3rd Joint US-European Fluids Engineering Summer Meeting and 8th International Conference on Nanochannels, Microchannels, and Minichannels
FEDSM-ICNMM2010
August 1-5, 2010, Montreal, Canada

FEDSM-ICNMM2010-30777

ANALYTICAL AND NUMERICAL STUDY OF A SWIRLING SUBMERGED JET FLOW

H. Alighanbari
Department of Aerospace
Engineering, Ryerson University
Toronto, ON, Canada, M5B 2K3
halighan@ryerson.ca

M.R. Amiralaei
Department of Aerospace
Engineering, Ryerson University
Toronto, ON, Canada, M5B 2K3
mamirala@ryerson.ca

S. Savtchenko
Department of Aerospace
Engineering, Ryerson University
Toronto, ON, Canada, M5B 2K3
Sserguei_1@hotmail.com

ABSTRACT

The present study is conducted to investigate the details and characteristics of swirling submerged jets when transferred into a system of helical vortices downstream in a bathtub-like flow. Both analytical and numerical results are presented. In the analytical solution, upstream flow is considered to be two-dimensional with piecewise-constant vorticity profile. The instability of such a flow leads to the formation of two-dimensional dipolar or tripolar vortical structures. It is shown that the size of the vortexless annular area inside the initial vortex is a critical parameter in the two dipolar unstable or tripolar stable structure formations, and that such tripolar flow transforms downstream to a three-dimensional steady helical vortex system, which rotates as a whole and propagates in the downstream direction. The mechanism of screwing vortex filaments into a steady system of helical vortices is also presented. The numerical simulations also confirm the initiation and generation of dipolar vortex structures.

INTRODUCTION

Vortex instability changes the flow structure in swirling motions and can generate different vortical patterns such as helical vortex structures. This instability and its behavior are affected by different parameters such as the geometric characteristics and swirling speed. In some instances, multi-vortex structures can contain axial flows in opposite directions, which add to the inherent complexity of the corresponding fluid dynamics. Natural vortex flows such as tornadoes are very good examples of this instability, which are formed and further developed into multi-vortex structures. Due to the inherent complexity of these instabilities, there is no explicit theoretical solution for swirling submerged jets.

Experimental studies are conducted to investigate the decay of swirling vortices into intertwined and multi-vortex structures [1 and 2]. The converted vortical structures can also be in the form of dipolar or tripolar configurations. Van Heijt et al. [3] examined the formation of tripolar vortices.

The vorticity profile and dynamics of uniform helical vortices were studied by some researchers [4-7]. However, the corresponding formation mechanism of these helical structures was not studied. Takaki and Hussain [8] showed that the straight and parallel vortex filaments cannot be screwed into a helix if their distance remains constant.

The present study is conducted to investigate the transformation process of initially axisymmetric swirling submerged jet flow into a system of helical vortex cores. Analytical method is used to study the development of a 2D swirling flow into a stationary fluid downstream. The formation of a 2D tripolar vortex system is demonstrated using the method of discrete vortex particles. A Computational Fluid Dynamics (CFD) study is also conducted to observe the formation of the dipolar vortex structures.

PROBLEM DEFINITION AND EXPERIMENTAL OBSERVATIONS

Figure 1 is the schematic of a chamber divided into two sections having a wall with a hole O (radius a = 10 mm) in the middle. The lower section is filled with an irrotational fluid, but the same fluid rotates in the upper section. Another hole O′ (radius 4 mm) in the bottom of the lower section is open to the atmosphere. Both holes are located on the same vertical axis of

symmetry. The horizontal size of each section (L = 860 mm) is much bigger than the radiuses of the holes. Both holes are opened at the same time, and consequently a vortex drain into the irrotational fluid is formed, which is called a swirl submerged jet. The axial flow velocity in the drain is kept approximately constant ($v_{zr_o} \approx$ 0.5 m/sec), but the radial velocity of the vortex draining $v_{\varphi r_o}$ into the hole O varies to 5 m/sec.

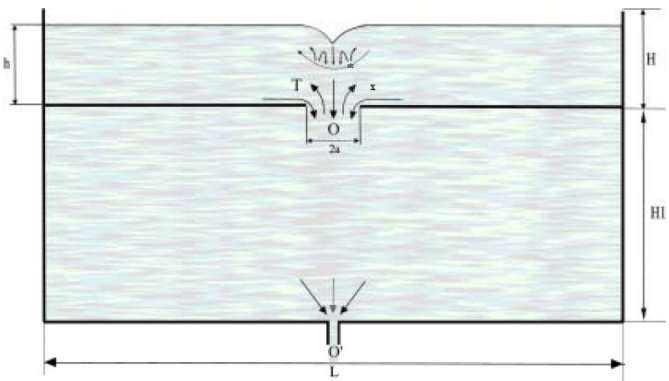

Fig. 1: Experimental set up.

Visualization has shown that above hole O and to some extent below it, the flow is always axisymmetric. Let's consider the flow above the hole. It is observed that the flow well outside the central area presumes a solid-body rotation at a low frequency (Ω). In most of the experiments, Ω has a value about 0.1 rad/sec. The respective vorticity ($\omega_o = 2\Omega$) is almost constant spatially as well as temporally. The azimuthal flow in the central drain area is complex, but for simplification we assume that it rotates like a solid body and has an average time dependent vorticity $\omega(t)$. Thus, in a rotational sense, the simplified flow model consists of two regions; a low rotational outer region and a high rotational central region. It is also assumed that the axial velocity in the outer region is negligible. Conversely, in the central region the flow is axial with no radial velocity. In the area between the outer and central regions, the flow makes a turn, which basically leads to stretching of the vortex lines. This leads to the so-called vorticity intensification.

It can be shown that such a model satisfies the basic flow characteristics such as the viscosity effect. The influence of viscosity is significant in the boundary layer on the solid walls and in the area between the central and outer regions around which relative rotation exists. The thickness of the rotational boundary layer on the walls is in the order of $\sqrt{\nu/\Omega}$ or about 3 mm, where ν is kinematic viscosity. The viscous central core radius can be estimated as $\sqrt{\nu h/Q}\, a$ which is less than 1 mm, where Q is the volume flow rate and h is the liquid level in the upper section (Fig. 1). Hence, above 3 mm of sectional wall and out of a thin layer between the outer and central regions, the flow may be considered as inviscid. Vortex line stretching causes the vorticity intensification. The vorticity in the outer region ω_{out} is constant, and the vorticity in the central region $\omega_c(t)$ is spatially constant, but increases with time.

Visualization is performed by inserting dye through a small square cross-sectional tube at point P. The tube axis is directed azimuthally. The process is shown schematically in Figure 2a, and the real experimental photo is represented in Figure 2b. The dye relative velocity is negligible, and the flow near the tube tip may be considered as a colored jet issuing with the same velocity as the liquid at the same location (Figure 2).

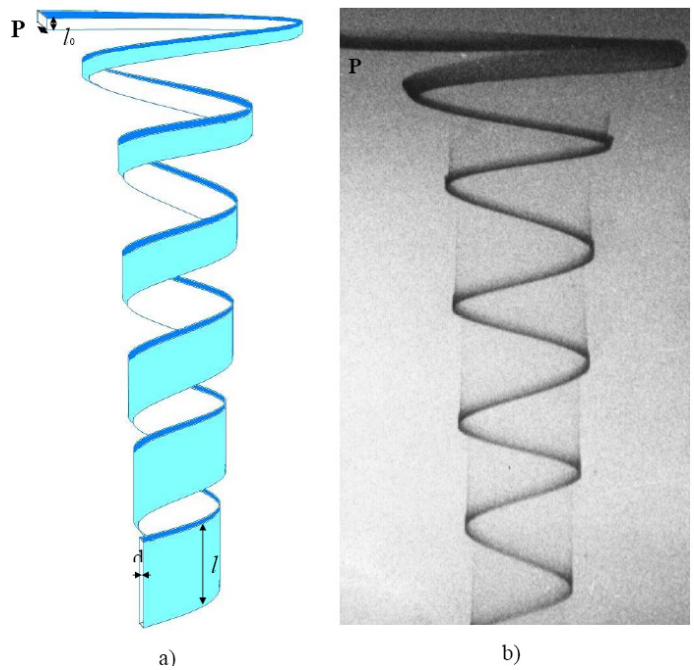

Fig. 2: The spreading of dye along the vortex surface, (a) schematic, (b) experimental.

The material elements of the flow are colorized when they pass through the cross-section of the tube tip. The instantaneous set of such elements continuously passing through the tip point visually looks like a colored jet issuing from the orifice. For simplicity one may represent such an orifice as a square with size l_0. One side of the square is directed axially and the other radially. It will be shown that such a jet transforms downstream to a thin tape coincident with the vortex surface. When a liquid element moves from its original location in the outer region to the central region, it stretches according to [9].

$$\frac{\omega_c(t)}{\omega_{out}} = \frac{l(t)}{l_0} \tag{1}$$

where l is the length of the jet cross-section in the axial direction.

The radial velocity is independent of the axial coordinate [10]. It means that the liquid particles located on cylindrical surfaces with certain radius R come to the central area at the same time. Taking into account the conservation of circulation:

$$\omega_c = \omega_0 + \frac{R^2}{a^2}\omega_0 \tag{2}$$

The conservation of mass gives:

$$R^2 = \frac{Q}{\pi h_{av}} \tag{3}$$

where $h_{av} = (h_0+h)/2$ is the average liquid level during which a cylindrical volume with radius R drains in the central area. Therefore:

$$\omega_c = \omega_0\left(1+\frac{Qt}{\pi h_{av}}\right) \tag{4}$$

Note that h_{av} is a weakly time dependent parameter. From Equations 1-4 and $h = h_0 - Q/\pi R^2_0$, in terms of the current liquid level h:

$$l = \left(1 + P\,\frac{1-\dfrac{h}{h_0}}{1+\dfrac{h}{h_0}}\right) l_0 \tag{5}$$

where $P = 2R^2_0/a^2$.

The thickness of the colored jet in the central area may be found by the conservation of mass. Taking into account that the two cross-sections of the jet are oriented in the azimuthal direction then:

$$l_0^2 v_{\varphi 1} = l d v_{\varphi a} \tag{6}$$

and

$$v_{\varphi 1} = \frac{\omega_0 R_1}{2} + \pi a^2 \omega_0\left(1+P\frac{1-h/h_0}{1+h/h_0}\right)/R_1 \tag{7}$$

where index 1 refers to the condition at the point where the tip of the dye tube is located. Using (6) and (7) one obtains:

$$\frac{d}{l_0} = \frac{R_1}{a}\frac{1}{\left(1+P\dfrac{1-h/h_0}{1+h/h_0}\right)^2} + \frac{\pi a}{R_1}\frac{1}{\left(1+P\dfrac{1-h/h_0}{1+h/h_0}\right)} \tag{8}$$

Using Equations 5 and 8, it can be estimated that an initially tiny square shaped colored jet with 1 mm size in the outer region is deformed in the central area to a film of about 2 cm width and 1 micron thickness, while the liquid level decreases about 10%. Equation 1 is vectorial, i.e., the material and vortex lines stretch in the same direction. Therefore, the film spreads out along the vortex surface.

Now, consider the flow below the hole O. The schematic of the flow near the hole O in the axial and azimutal planes are presented in Figures 3a and 3b, respectively. The central vortex with positive vorticity is concentrated in area A (Figure 3a), and the black spot (Figure 3b). A negative vorticity in the area C′ is formed from the downward boundary layer of the rotational motion above the middle wall (area B).

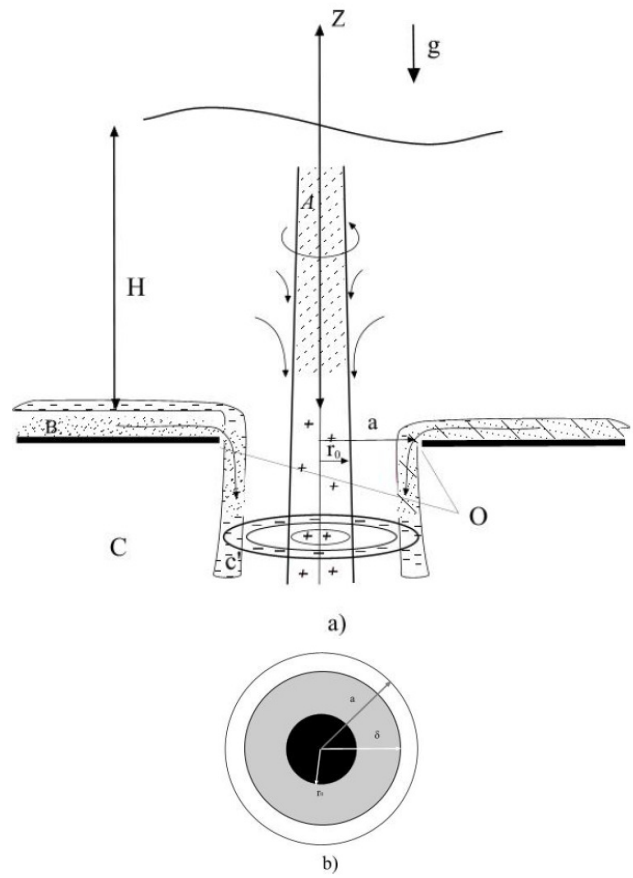

Fig. 3: Schematic picture of the flow near the orifice.

The negative vorticity is the white area shown in Figure 2b. The resultant circulation is zero around the circle that encompasses both areas. Further, we assume that in the A and C′ regions the vorticity is distributed uniformly. In general, there is some gap with zero vorticity between regions A and C′. This is a free vortex area and an example of the compensated Rankin vortex. The radius of the central vortex can be obtained approximately from the integral form of the continuity equation.

$$r_0 \Delta v_z \approx 2h v_{r0} \tag{9}$$

where v_{r0} is the radial velocity on the edge of the central vortex area and

$$\Delta v_z \approx v_z \tag{10}$$

The radial velocity increases from zero on the axis to the same order as the axial velocity outside the hole, but still it should be much less on the edge of the high vorticity central area $v_{r0} << v_z$. Let's assume that radial velocity on the edge is one order of magnitude less than the axial velocity $v_{r0} = v_z/10$. At large radius, the radial velocity reaches the same order of

magnitude as the axial velocity. From (9) and (10) one may obtain:

$$r_0 \approx 0.2h \tag{11}$$

The observations show that the flow instability is developed downstream spatially. Thus, the disturbances grow downstream and form a new structure; while in each cross-section the flow is steady.

When both holes are opened, the draining vortex begins to intensify slowly versus time and level h. For a wide range of parameters, it is observed that the primary axisymmetrical rotational flow (schematically shown in Figure 3) transforms into a secondary vortex structure of the double helix type.

Two regimes have been investigated in detail for h= 5 cm and h=2.5 cm. The rotational velocity profile of the draining vortex is analyzed visually by looking at the shape of the free liquid surface in the upper section. For the h = 5 cm case, the inner solid-rotational core (black area in Figure 3) fills almost the entire hole O according to (11). This corresponds to a situation with no or a small gap (inner gray area) in Figure 3. In the second case, as follows from (11), the inner solid-rotational core has a radius sufficiently less than the size of the hole O. This corresponds to a situation with a large gap (inner gray area) in Figure 3.

ANALYTICAL SIMULATION METHOD

In the preceding section, we assumed that the vorticity above hole O is piece-wise constant. The characteristics of the vorticity under hole O is investigated in detail in the following section, assuming two-dimensional flow under hole O.

The method of discrete vortex particles is employed here to study the development of the unstable annular shear flows with respect to two-dimensional disturbances. A two-dimensional instability mechanism is assumed here for this class of flows. Such an approximation can be justified by the fact that according to the Squire theorem most of the unstable disturbances are two-dimensional. Moreover, it is assumed that the fluid is ideal.

Based on the two-dimensional assumption, the stability of the vortex flow can be analyzed through the analysis of properties of the flow cross sections. Selection of the cross sections depends on the problem. The development of instability for the swirl flow passing through irrotational fluid was presented in the former section, and it was shown that the irrotational outer fluid goes aside and surrounds the incoming rotational liquid (area C in Figure 3). The size of the potential part (between C′ and A) is zero, or is of the same order of magnitude as the size of vortex area (A). This flow may be modeled as a compensated Rankin vortex. The positive vorticity of the initial flow is uniformly distributed inside the circular core with radius r_0 (dark spot in Figure 3b). The negative vorticity is uniformly distributed inside the annular layer with inner and outer radiuses δ and a, respectively (white ring in Figure 3b). The low vorticity liquid is located outside the vortex and inside the annular gap between the positive and negative regions (gray area in Figure 3b).The vorticity inside the gap is ignored. The early stage of instability of a similar flow was studied by Carton et al. [11]. However, they assumed a flow with smooth profile. The initiation of a tripolar vortex structure was observed at the first stage of instability development. The detailed analysis was provided for one vorticity profile. The calculations were made up to tripolar structure formation. The development of such tripoles over a greater period of time was studied by Kloosterziel and Carnevale [12]. They studied the development of instability for the smooth initial profiles, and showed that different types of multi-vortex structures are formed depending on the initial vorticity profile. They observed tripolar structure for certain type of profiles, and showed that the tripolar structure is conserved for time sufficiently longer than its formation period. However, no criteria were found for tripolar or two dipolar regimes. In the present study, a different analytical method is employed to investigate the instability of the compensated piecewise-uniform vorticity distribution. It is shown that the size of the vortexless area inside the complex vortex is a critical parameter for either tripolar or two dipolar regime realization.

In this paper, the method of vortex dynamics [13] is used. The vorticity field is simulated by a set of discrete vortex particles with Gaussian distribution. The equations of motion of vortex particles are as the following:

$$\frac{dx_\alpha}{dt} = -\frac{1}{2\pi}\sum_{\beta=1}^{N}\Gamma_\beta\left[1-\exp\left(-\frac{r_{\alpha\beta}^2}{\sigma_\alpha^2+\sigma_\beta^2}\right)\right]\frac{\left(y_\alpha - y_\beta\right)}{r_{\alpha\beta}^2},$$
$$\frac{dy_\alpha}{dt} = \frac{1}{2\pi}\sum_{\beta=1}^{N}\Gamma_\beta\left[1-\exp\left(-\frac{r_{\alpha\beta}^2}{\sigma_\alpha^2+\sigma_\beta^2}\right)\right]\frac{\left(x_\alpha - x_\beta\right)}{r_{\alpha\beta}^2} \tag{12}$$

where $r_\alpha = (x_\alpha, y_\alpha)$ is the radius-vector determining the position of the vortex particle center α on the x, y plane; σ^2_α is the distribution of the vortex particle vorticity; Γ_α is the circulation of the particle vorticity. The dispersion of the vortex particle is determined subject to the condition of the best approximation of the initial vorticity field.

The system described by Equations 12 is conservative. In this system as in the initial continual one, the laws of conservation of momentum, angular momentum, and energy are satisfied. In the calculations, the initial arrangement of vortices was specified in such a way that the grid formed by them on the plane had the identical area of the cells. In this case, the vorticity distribution is uniform. Thus, the initial problem of evolution in the disturbed field of vorticity is reduced to the solution of Eqs. 12, under the specified initial conditions. The equations were solved by the fourth-order Runge-Kutta method. The accuracy was controlled by the fulfillment of the conservation laws. Several thousands of elementary vortex particles were used in the calculations. The circulation of the central vortex is taken as 2Γ. The unit value of time T in this paper is the rotation time of the Rankin vortex with radius a and

circulation Γ. The rotational velocity on the vortex boundary is $v_R = \Gamma/4\pi a$. Hence, T may be expressed by:

$$T = 4\pi a^2 / \Gamma \tag{13}$$

An analytical study of temporal instability is provided in Figure 4 for similar flow as in Figure 3.

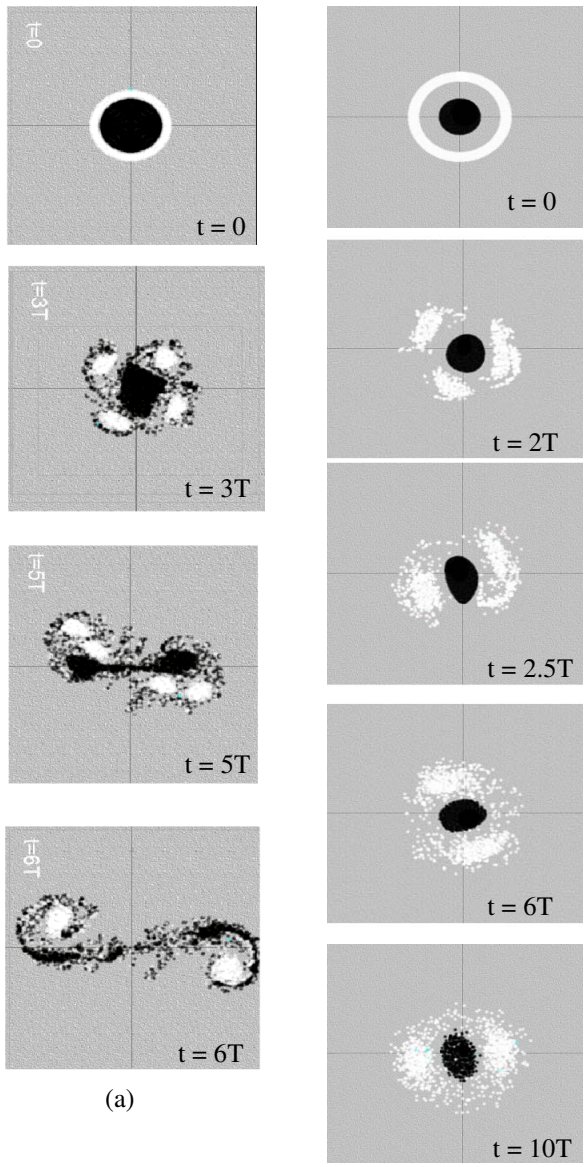

(a) (b)

Fig. 4: Numerical results (black: positive vorticity, white: negative vorticity, grey: no vorticity). a) development of instability when there is no inside vortexless gap.
(b) development of instability when inside vortexless gap is sufficiently wide.

As mentioned before, the instability in the presented experiments is spatial. In the laboratory frame of reference the flow is steady. Thus, each liquid particle coming down from the orifice O reaches some location z at the same time t as any other particle. Further, it is assumed that the flow is flat on this phase of analysis, i.e. axial velocity is not dependent on the radial coordinate. In its own frame of reference the instability of each liquid particle develops temporally. It means that for each location along z one may introduce a corresponding moment of time in the calculation track. Thus, each consequent series of the flow pictures in the experiment along z corresponds to some analytical set made in temporal analysis. This comparison is qualitative because the three-dimensionality becomes significant after a short distance downstream. It was found that if either no gap or a small enough gap between the two areas of vorticity exists, the central vortex is destroyed (Figure 4a) and two dipolar vortices are formed. They continue rotating as a whole around an axis of symmetry and move in opposite radial directions. Thus, the initial vortex breaks down. This analytical situation is in agreement with the experimental one where the vortex structure is short and expands quickly. If the gap is wide enough, the lateral vortices do not move from the central vortex, and the central vortex does not break down. Instead, they rotate around the central core for a period of time sufficiently longer than the formation period. The detailed analytical study shows that the steady tripolar structure is formed when the width of the gap is larger than approximately the radius of the central core. Two-dipolar structures are formed for smaller gaps ($\delta - r_0 < r_0$). This analytical situation qualitatively is in agreement with the experiment where the vortex structure is long and expands slowly. This shows qualitative correlation between analytical and experimental results. It is also shown that the existence of a wide enough gap in vorticity inside the complex vortex leads to the formation of a long and compact tripolar structure. The presence of the wide enough low vorticity area inside the vortex leads to similar results (Kloosterziel and Carnevale [12]) as in Figure 4b. Thus, one can conclude that the presence of a wide enough low vorticity annular area inside the compensated vortex leads to stable tripolar structure formation.

NUMERICAL SIMULATION METHOD

Three-dimensional Navier-Stokes equations are used, which are presented in the following non-dimensional form:

$$\frac{\partial u}{\partial x} + \frac{\partial v}{\partial y} + \frac{\partial w}{\partial z} = 0$$

$$\frac{\partial u}{\partial t} + u\frac{\partial u}{\partial x} + v\frac{\partial u}{\partial y} + w\frac{\partial u}{\partial z} = -\frac{\partial p}{\partial x} + \frac{1}{\mathrm{Re}}\left(\frac{\partial^2 u}{\partial x^2} + \frac{\partial^2 u}{\partial y^2} + \frac{\partial^2 u}{\partial z^2}\right) \tag{14}$$

$$\frac{\partial v}{\partial t} + u\frac{\partial v}{\partial x} + v\frac{\partial v}{\partial y} + w\frac{\partial v}{\partial z} = -\frac{\partial p}{\partial y} + \frac{1}{\mathrm{Re}}\left(\frac{\partial^2 v}{\partial x^2} + \frac{\partial^2 v}{\partial y^2} + \frac{\partial^2 v}{\partial z^2}\right)$$

$$\frac{\partial w}{\partial t} + u\frac{\partial w}{\partial x} + v\frac{\partial w}{\partial y} + w\frac{\partial w}{\partial z} = -\frac{\partial p}{\partial z} + \frac{1}{\mathrm{Re}}\left(\frac{\partial^2 w}{\partial x^2} + \frac{\partial^2 w}{\partial y^2} + \frac{\partial^2 w}{\partial z^2}\right)$$

where u, v, w, and p are the non-dimensional velocities and pressure, respectively, t is the physical time, and Re stands for the Reynolds number.

The existing numerical simulation is conducted to examine the early stages of vortex instability and generation of the dipolar vortical structures, discussed in the theory section. Hence, constant axial velocity (u_z = 0.5 m/s) and rotational speed (Ω = 0.1 rad/s) with no radial velocity (u_r = 0) are utilized at the inlet. Moreover, the inlet conditions are set to match the first case studied in the analytical part, no vortexless area. Figure 5 shows the schematic of the simulated 3D tank and the applied boundary conditions. The outlet is set to atmospheric pressure while its velocity is obtained using a zero-gradient boundary condition during the simulations. The tank side-walls are set to 43a (a is the radius of the inlet) from the centre line. Hence, the undesired effects from the tank walls on the vortex development are minimized.

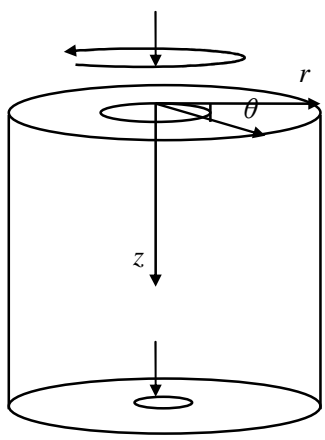

Figure 5: Schematic of the computational domain and the applied boundary conditions

O-type mesh is used in the radial direction and the mesh is graded near the inlet boundary. Figs. 6a-c show the dipolar vortex formation at three different heights (at the same time) measured from the inlet (where z = 0). The figures are in qualitative agreement with the predictions of the analytical method shown above. It should be mentioned that the top view of the simulated tank is shown in Figs. 6a-c. The white area shows the outer rotational area which has a negative rotational speed with respect to the positive rotating fluid shown by the black area.

The total number of cells was 50×10^3 which was obtained after extensive grid-sensitivity analyses. The computations utilize a second order central differencing scheme for convective and diffusive terms using a steady state approach. The resulting linear system of equations is treated with Preconditioned Conjugate Gradient (PCG) solvers, and the Pressure Implicit and Splitting of Operators (PISO) algorithm is used for the pressure-velocity coupling. The computations are carried out in OpenFOAM [14].

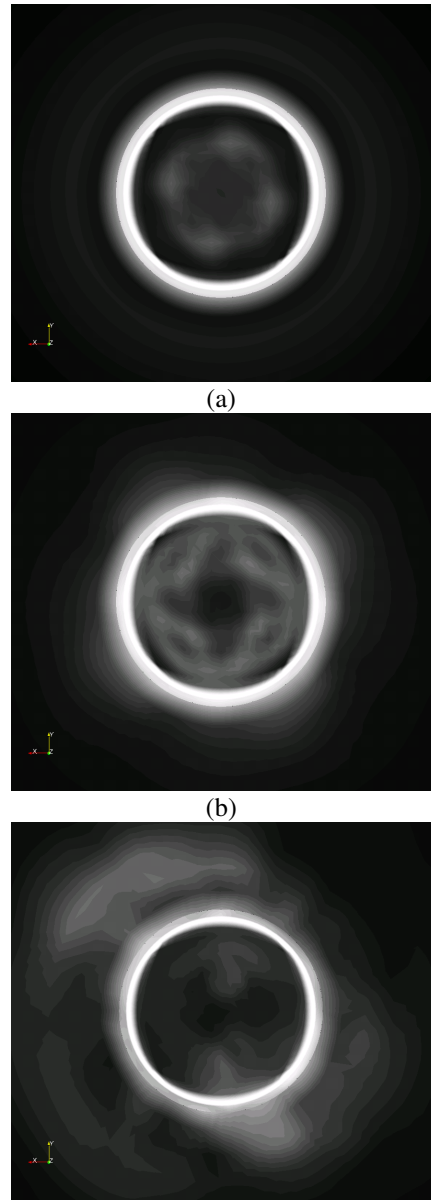

Fig. 6: Early stages of the formation of dipolar vortex structures

CONCLUSION

Development of unstable swirl submerged jet into a downstream stationary fluid is investigated both analytically and numerically. The analytical study is based on two-dimensional and piecewise constant vorticity profile, and the method of vortex dynamics is the utilized approach. It is shown that a system of two dipolar unstable or tripolar stable secondary vortices is formed as a result of the two-dimensional instability of the swirl axisymmetrical flow. It is also observed that the existence of the vortexless annular region is a critical

factor in obtaining dipolar or tripolar vortex structures. Different parameters, such as free liquid level, influence the size of the vortexless region. In the case of the tripolar structures, they can be transferred and converted into three-dimensional helical structures. The helical vortices are sufficiently longer, more compact, and uniform downstream than the developed structures downstream when dipolar vortices are formed. The numerical results also verify the early formation of the dipolar vortex structures.

ACKNOWLEDGEMENT

The authors gratefully acknowledge the financial support of the Natural Sciences and Engineering Council of Canada (NSERC)

REFERENCES

[1] Lugovtsov, B. A., "Laboratory Models of the Tornado-Like Vortices, " In book "Intense Atmospheric Vortices," Editors: Bengtsson, L., Lighhill, M. I., Springer-Verlag, 1982.

[2] Fujita, T. T., The Lubbock Tornadoes; a Study of Suction Spots, Weatherwise, 23, 1970.

[3] Van Heijst, G. J. F., Kloosterziel, R. C., Williams, C.W.M., "Laboratory Experiments on the Tripolar Vortex in a Rotating Fluid," *J. Fluid Mech.*, Vol. 225, 1991, pp. 301-331.

[4] Hardin, J. C., "The Velocity Field Induced by a Helical Vortex Filament," *Physics of Fluids*, Vol. 25, 1982, pp. 1949-1952.

[5] Ricca, R. L., "The Effect of Torsion on the Motion of a Helical Vortex Filament," *J. Fluid Mech.*, Vol. 273, 1994, pp. 241-259.

[6] Alekseenko, S. V., Kuibin, P. A., Okulov, V. L., Shtork, S. I., "Helical Vortices in Swirl Flow," *J. Fluid Mech.*, Vol. 382, 1999, pp. 195-243.

[7] Wood, D. H., Boersma, J., "On the Motion of Multiple Helical Vortcies," *J. Fluid Mech.*, Vol. 447, 2001, pp. 149-171.

[8] Takaki, R., Hussain, A. K. M. F., "Dynamics of Entangled Vortex Filaments," *Physics of Fluids*, Vol. 27, 1984, pp. 761-763.

[9] Batchelor, G.K.1970. An Introduction to Fluid Dynamics, Cambridge University Press.

[10] Lewellen, W.S., 1962. A solution for three-dimentional vortex flows with strong circulation, J. Fluid Mech.,14, 420-433.

[11] Carton, X.J., Flierl, G.R., Polvani, L.M.1989. The generation of tripoles from unstable axisymmetric isolated vortex structures, Europhys. Lett., 9, 339-344.

[12] Kloosterziel, R.C., Carnevale, G.F, 1999. On the evolution and saturation of instabilities of two-dimensional isolated circular vortices, J. Fluid Mech., 388, 217-257.

[13] Veretentsev, A.N., Ya Rudyak, V., Yanenko, N.N., 1986. Construction of discrete vortex models of ideal incompressible-fluid flows, Zhurnal Vychislitel'noi Matematiki Matematicheskoi Fiziki, 26(1), 103-112.

[14] OpenFOAM, the Open Source CFD Toolbox, User Guide, version 1.4.1, August 2007.